WAVEGUIDE TECHNIQUES FOR INTEGRATED OPTICS

W. M. Caton, et al

Naval Electronics Laboratory

Prepared for:

Advanced Research Projects Agency

30 January 1974

WAVEGUIDE TECHNIQUES FOR INTEGRATED OPTICS

Progress is reported in five areas; for example, patterns for direct optical waveguides have been fabricated in different materials by electron beam exposure of electron resist

W. M. Caton and T. G. Pavlopoulos

Research and Development

30 January 1974

NAVAL ELECTRONICS LABORATORY CENTER
SAN DIEGO, CALIFORNIA 92152

UNCLASSIFIED

Security Classification

DOCUMENT CONTROL DATA · R & D

Security classification of title, body of abstract and indexing annotation must be entered when the overall report is classified

1 ORIGINATING ACTIVITY (Corporate author) Naval Electronics Laboratory Center San Diego, California 92152	2a. REPORT SECURITY CLASSIFICATION UNCLASSIFIED 2b GROUP

3 REPORT TITLE

WAVEGUIDE TECHNIQUES FOR INTEGRATED OPTICS

4 DESCRIPTIVE NOTES (Type of report and inclusive dates)

Research and Development — 1 April to 30 September 1973

5 AUTHOR(S) (First name, middle initial, last name)

W. M. Caton and T. G. Pavlopoulos

6 REPORT DATE 30 January 1974	7a. TOTAL NO OF PAGES	7b. NO OF REFS 14
8a CONTRACT OR GRANT NO b. PROJECT NO ARPA (NELC F215) c. d.	9a. ORIGINATOR'S REPORT NUMBER(S) NELC TR 1909 9b. OTHER REPORT NO(S) (Any other numbers that may be assigned this report)	

10 DISTRIBUTION STATEMENT

Approved for public release; distribution unlimited

11 SUPPLEMENTARY NOTES	12 SPONSORING MILITARY ACTIVITY Advanced Research Projects Agency

13 ABSTRACT

The advancement of integrated optics circuits and fiber optics with a view to their application in Navy and other DoD systems is the objective of this ARPA-sponsored NELC program. This report documents progress in a number of areas. Patterns for direct optical waveguides have been fabricated in different materials by electron beam exposure of electron resist (DIFFUSION MASK FABRICATION); studies have been performed on the efficiency of planar horn-shaped regions in waveguides as coupling devices (THEORETICAL INVESTIGATION OF COUPLING TO WAVEGUIDES WITH LINEARLY TAPERED HORNS); an electron beam microscope has been used to measure the variation in the concentration of the electrically active impurities in laser diodes and other semiconductor structures (ELECTRON BEAM MICROPROBE); an apparatus has been constructed for the measurement of the refractive index of thin films (DETERMINATION OF THE REFRACTIVE INDEX OF THIN DIELECTRIC FILMS); and low-loss channel waveguides have been produced by focusing an argon ion cw laser with the aid of a microscopic objective on the surface of a piece of highly absorbing glass (CW LASER-FABRICATED CHANNEL ACTIVE AND PASSIVE OPTICAL WAVEGUIDES).

DD FORM 1 NOV 65 1473 (PAGE 1)

0102-014-6600

UNCLASSIFIED

Security Classification

14 KEY WORDS	LINK A		LINK B		LINK C	
	ROLE	WT	ROLE	WT	ROLE	WT
Integrated optics						
Optical waveguides						
Fiber optics						
Optical coupling						
Thin films – Optical properties						
Integrated optic circuits – Fabrication						

PROBLEM

Study and contribute to the advancement of integrated optical circuits (IOCs) and fiber optics and their application in communication systems. Emphasize applications in Navy and other DoD programs in aircraft, shipboard, and other systems.

Contribute to and evaluate the state of the art in material and device techniques for the fabrication of IOC devices such as couplers, switches, and modulators. Determine the feasibility of employing fiber optics and IOC technology in military applications such as high-capacity (multi-GHz) telecommunications and secure (nonradiating and radiation-resistant) communication systems.

RESULTS

1. Patterns for direct optical waveguides have been fabricated in different materials by electron beam exposure of electron resist.

2. Theoretical studies have been performed on the efficiency of planar horn-shaped regions in waveguides as coupling devices.

3. An electron microscope has been used to measure the variation in the concentration of the electrically active impurities in laser diodes and other semiconductor structures.

4. An apparatus has been constructed for the measurement of the refractive index of thin films. The equipment will be employed for the determination of refractive indexes of thin dielectric films and semiconductor surfaces such as channel optical guides produced by diffusion into ZnSe. It will also be used to measure the refractive index of sputtered glass film waveguides.

5. Low-loss channel waveguides have been produced by focusing an argon ion cw laser with the aid of a microscopic objective on the surface of a piece of highly absorbing glass. At the laser beam focal point, glass is evaporated and grooves 2–10 μm wide are produced.

RECOMMENDATIONS

1. Continue the development of techniques for fabricating prototypes of IO components emphasizing single-mode waveguides.

2. Demonstrate coupling in waveguides as a first step in the development of IOC switches; develop high-efficiency couplers, switches, modulators, and other IOC components.

3. Set up a program for the improvement and refinement of methods of fabricating IOC components; develop the capability of producing small structures to tolerances of fractions of micrometers.

ADMINISTRATIVE INFORMATION

The work reported here was sponsored by the Advanced Research Projects Agency, Material Sciences, Arlington, Virginia, under ARPA Order 2158, Amendment 1; Program Code 3010; Contract F215.01 (NELC F215). Work was performed from 1 April to 30 September 1973. Principal investigator was D. J. Albares of NELC Electro-Optics Technology Division (Code 2500); associate investigators were W. M. Caton, D. B. Hall, W. E. Martin, T. G. Pavlopoulos, and H. F. Taylor of Code 2500, H. H. Wieder of Electronic Materials Science Division (Code 2600), J. H. Harris of the University of Washington; C. Yeh of the University of California at Los Angeles; and R. B. Wilson of the Hughes Research Laboratories, Malibu, California. This report was authored by Caton and Pavlopoulos, and was approved for publication 30 January 1974.

CONTENTS

REVERSE SIDE BLANK

INTRODUCTION

The fabrication of miniature solid-state optical components and thin-film waveguides to interconnect them on semiconductor or dielectric substrates is becoming feasible with the advancement of such disciplines as the materials sciences, quantum electronics, and guided-wave optics. Integrated optical components – sources, detectors, modulators, and various coupling elements – on one or more tiny substrates will comprise systems much smaller in size and weight than optical systems employing discrete components. The new systems will be much less susceptible to environmental hazards, such as mechanical vibrations, extremes in temperature, and electromagnetic fluctuations, because of their small size and packaging density. In addition, wideband active components, such as waveguide electrooptic modulators, will be able to operate at very low power levels because of the small dimensions involved.

Integrated optics will perform a number of functions in the area of optical communications. They include rapid modulation and switching by guided-wave elements using applied fields to generate small electrooptic or magnetooptic index changes, coupling, filtering of signals, light detection by p-n junctions or other structures in thin films, and light generation by thin-film laser elements.

Guided-wave optical components have found an important potential use in the area of optical communications because of the recent progress in the fabrication of single-mode figer-optic waveguides with very low losses. Fiber-optic waveguides with losses as low as 4 dB/km at 0.85-μm and 1.06-μm wavelengths (for GaAs and Nd-YAG lasers, respectively) and with single-mode fibers having anticipated bandwidths as high as 10 GHz for a 1-km length immensely widen the horizon of optical communications. However, devices must be developed to couple energy efficiently with the fibers and to process the optical information efficiently at rates approaching the bandwidth capacity of the fibers.

Another promising area is in fast, high-capacity, high-density multiport switches for interconnecting networks.

Fiber-optic waveguide systems offer significant advantages for military information transfer, both immediately, with discrete components and multimode fibers, and in the future, with single-mode fibers and integrated optical elements. These advantages include freedom from electromagnetic interference (EMI), elimination of grounding problems, and increased security (no signal leakage), as well as the potential for large savings in size, weight, power consumption, and cost. In addition to high-capacity point-to-point communications, a major interest in integrated optics from a military stand-point is the potential for implementing a fiber-optic-transmission-line, multi-terminal (data bus) multiplexing system through low-loss coupling and modulation elements. This will provide isolated-terminal, redundant information transfer, thus facilitating the truly modular (including distributed computer) command control and communications system.

The objective of the program reported here is to advance the material and device physics of integrated optics for military applications, to establish in concert with other Navy and DoD programs a continuing assessment of system requirements and cost benefits for R&D investments in each application area, and to produce prototype optical elements and subsystems that

are aimed at satisfying these requirements. The work on the program that was performed at Naval Electronics Laboratory Center (NELC) and on contracts administered by NELC was in the areas of integrated-optical-circuit (IOC) applications assessment, materials for IOC devices and substrates, pattern fabrication, theoretical analysis, components, and system concepts.

Experimentally, effort continued to be centered on the fabrication of IO components, such as optical waveguides and waveguide modulators. The reason for this concentrated effort in novel fabrication methods for optical waveguides and derived structures is that the employment of IOCs will be of practical interest only after inexpensive fabrication techniques have been developed.

This report is divided into the following six sections:

1. Application assessment.

2. Diffusion mask fabrication using a scanning electron microscope. Hughes Research Laboratories continued with their task of producing patterns for optical waveguide fabrication by electron beam exposure of electron resist on SiO_2 layers.

3. Theoretical investigation of coupling to waveguides with linearly tapered horns. J. H. Harris, University of Washington, theoretically considered the efficiency of coupling light into and out of waveguides by linearly tapered horns.

4. Electron beam microprobe. An electron beam microprobe was developed to determine parameters such as concentrations of impurities and mobilities in semiconductor devices (diodes).

5. Apparatus for the determination of the refractive index of thin dielectric films. An interferometric method to measure the refractive index of thin films is of special interest to the NELC effort in IOCs. Optical wave guiding is dependent on changes in the index of refraction.

6. Cw laser-fabricated channel active and passive optical waveguides. To the cadmium-diffused ZnSe waveguide structures, cw laser-fabricated waveguides were added.

Some of the material presented in this report is discussed in greater detail in the appendix.

APPLICATION ASSESSMENT

It is becoming widely accepted that fiber optics will ultimately be used in a variety of military information transfer applications. However, with present-day components (LED sources, multimode fiber bundles, PIN detectors), the important functions of switching, carrier-frequency multiplexing, and low-loss access ("tee") coupling are available only to a very limited extent. Since these are functions which are present in systems using electrical transmission lines, their loss or restriction is an important disadvantage in using fiber optics. It is anticipated that integrated optics components which will restore these capabilities in fiber optics systems can be developed;

indeed, their development is now underway at several laboratories, including NELC. From the standpoint of DoD, the restoration of these capabilities may be more important than the increased bandwidth capability provided by integrated optics.

The following table gives quantitative estimates (of a preliminary nature at this point) of the capabilities of present optical components vs IOCs and single-mode fibers, as well as examples of applications in which the IOC capabilities can be utilized.

		Present	IOCs	Applications
1.	Multipole switching			
	a. Speed	10^{-3} s	10^{-9} s	Centralized shipboard data transfer network.
	b. Number of terminals	8	128	Computer-sensor and computer-display links.

Present: LED switching using motion of prism for frustrated total internal reflection. Speed limited by inertia of mechanical system; number of terminals limited by losses and beam divergence.

IOCs: 7-stage switch composed of binary electrooptic elements on a 1-cm^2 substrate. Number of terminals limited by substrate size; speed limited by capacitance and power requirements.

2.	Access couplers			
	a. Loss	3 dB	½ dB	Avionics data bus. Shipboard data bus.
	b. Number of terminals without repeater	10	50	

Present: Glass block with internal mirror. Losses due to packing fraction and scattering at interface between fiber bundles and couplers. Number of terminals limited by minimum detectable signal level.

IOCs: Single-fiber to thin-film couplers. Losses due to reflection and misalignment at fiber-coupler interfaces. Number of terminals determined by minimum detectable signal level.

3.	Carrier-frequency multiplexing			
	a. Number of frequencies	5	50	AADC data bus. Shipboard data bus.
	b. Loss	5 dB	½ dB	Parallel data transfer.

TABLE (Continued)

	Present	IOCs	Applications
Present:	Glass block with multilayer interference coating. Losses due to poor filter selectivity add to losses at fiber bundle-to-coupler interface. Number of frequencies limited by spectral width of LEDs.		
IOCs:	Parallel waveguide coupled by periodic perturbations. Losses due to reflection and misalignment at fiber-coupler interfaces. Number of frequencies limited by thermal tuning of laser sources.		
4. Bandwidth			
a. Short lengths	50 MHz	10 GHz	Interbase communications. Phase comparison of radar signals.
b. Long lengths	100 MHz/km	10 GHz/km	Ground transmission of satellite data.
Present:	Bandwidth limited by LED response for short lengths; by multipath propagation for long lengths (> 2 km).		
IOCs:	Bandwidth limited by modulator response for short lengths; by material dispersion for longer lengths (> 1 km).		

DIFFUSION MASK FABRICATION USING A SCANNING ELECTRON MICROSCOPE

The scanning electron microscope at the Hughes Research Laboratories has been employed to fabricate SiO_2 masks for the production of optical waveguides in ZnSe. The masks are formed by electron beam exposure of resist and ion beam machining and/or chemical etching of the SiO_2 layer on the ZnSe substrate. These patterns comprise sets of three parallel lines of lengths from 1 to 5 mm, with widths of 4.5 μm and spacing of 2 μm.

Four samples of ZnSe, each with a 1000-Å layer of sputter-deposited SiO_2, were supplied by NELC. These samples were complicated by the presence of several large crystals terminating in the surface. Some of these crystal surfaces etched preferentially rough. The patterns were delineated as much as possible in the smooth areas between such surface structures, which were usually confined to a particular crystallite. However, in some cases the patterns intercepted such structures.

Chemical etching was employed after the electron beam exposure and development of the electron resist. This decision was based on successful results in the past. The validity of the choice is shown in figure 1, which is a scanning electron micrograph of a typical set of three etch channels in the SiO_2 films. Note that the edge roughness is undetectable, even at this magnification (probably $\leq$ 500 Å).

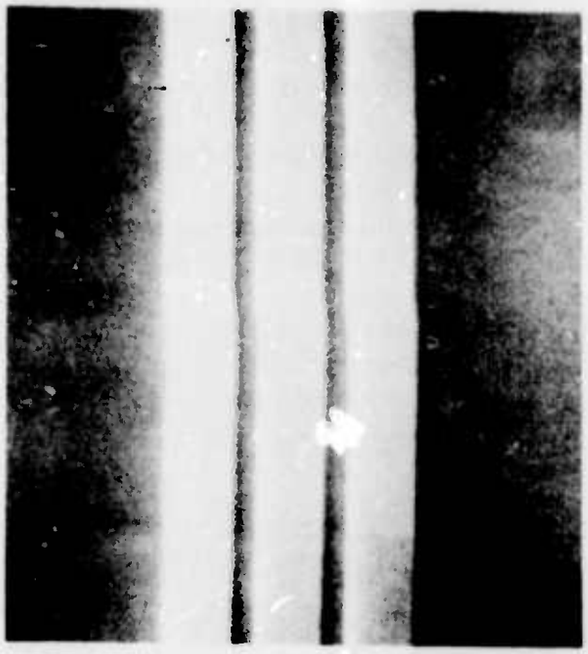

Figure 1. Scanning electron micrograph (2000x) of chemically etched channels in SiO_2. Channel width is 4.5 μm. Edge smoothness is probably less than 500 Å.

Only three of the four samples were deemed usable. Several sets of three parallel lines (many were more than 15 mm in length). were etched into the oxide layer of each sample. A photomicrograph of a typical line set is shown in figure 2.

Figure 2. Reflection photomicrograph (500x) of typical NELC sample. Lines pass through many surface irregularities (discussed in text). Photograph is typical of all line sets on this sample.

Linewidth control will improve as the optimum etch conditions are determined. The first sample produced showed significant undercutting, and it was found that sputter-deposited SiO_2 etches much faster than thermally grown SiO_2.

However, the later results for NELC No. 3 showed the etch under much better control and the linewidth more nearly equal to line separation.

Figure 1 reveals a problem that will need to be resolved in order to prevent light scattering out of the guides. The jog in the line set may be caused by stage translation during exposure, or more likely by specimen charging which momentarily deflects the electron beam. The latter cause can be eliminated by coating the resist with an electrically conductive film. If the problem is associated with stage instabilities, a more serious situation exists.

THEORETICAL INVESTIGATION OF COUPLING TO OPTICAL WAVEGUIDES WITH LINEARLY TAPERED HORNS

One of the design areas in integrated optics that generate conflicting requirements is the fabrication of modulators and switches. On one hand, the figure of merit (the ratio of drive power at center frequency to bandwidth) of modulators improves as the device size is reduced to micrometer and even submicrometer dimensions. On the other hand, the optical insertion loss problem generally worsens with reduced size. Insertion loss is attributable to several factors. Among these are the geometric factors of wall roughness and input and output coupling. This section is concerned with an aspect of the coupling problem.

We have investigated the efficiency of planar horn-shaped regions as coupling devices. The method of approach is to consider the reciprocal problem of mode conversion in an expanding planar horn. The narrow end of the horn has a cross section that conforms to a narrow linear waveguide and supports a single TE mode. It is assumed that this mode is launched at the narrow end of the horn. Progression of the mode along the horn is examined. As the wave propagates to larger horn widths, energy is coupled to higher-order modes. Coupling is restricted to modes of alternate order.

When the power distribution among the modes at the mouth of the horn is established, the coupling efficiency of an incident guided mode may be computed from the relation

$$\frac{P_c}{P_{in}} = \left|\int g_n(x,y)h(x,y)\,dx\,dy\right|^2 \frac{P_n}{P_o}. \qquad (1)$$

In this expression P_c/P_{in} is the power coupled into the linear waveguide relative to the incident power, P_n/P_o is the power in the n^{th} mode relative to the incident power as determined by the solution of the reciprocal problem, $g_n(x,y)$ is the normalized ($\int|g|^2\,dx\,dy = 1$) distribution of the tangential electric field at the mouth of the horn, and $h(x,y)$ is the normalized tangential electric field of the incident wave. The ratio P_n/P_o is shown in figure 3(A–L).

In the usual situation the guided plane waveguide mode has a spatial distribution $h(x,y)$ that is of modal character in the direction normal to the

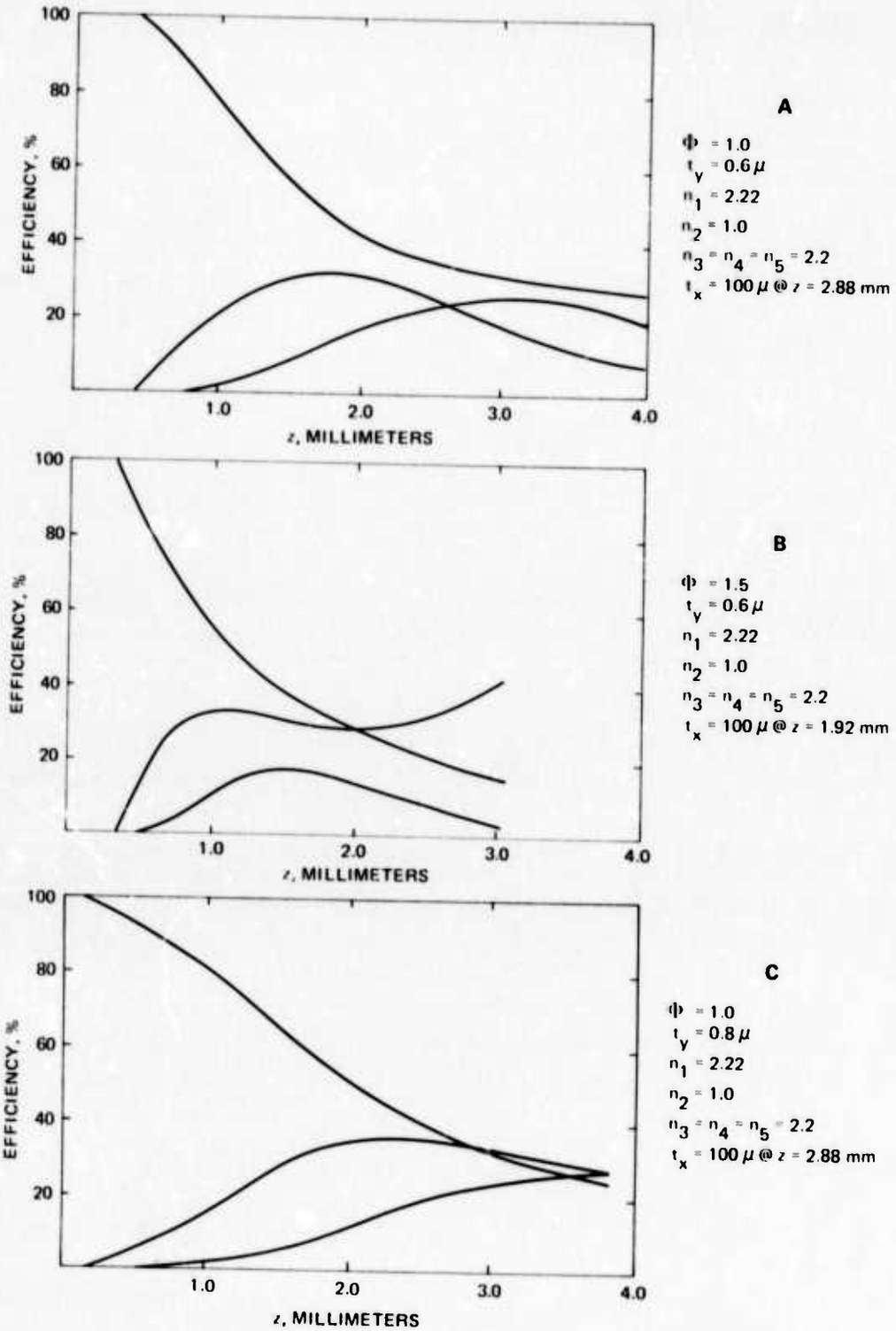

Figure 3. The power in modes of order zero, two, and four in an expanding planar waveguide horn vs distance z along the horn axis. The height of the planar horn is t_y, the index is n_1, and the guide is embedded in a region with n_2 above, n_4 below, and n_3 and n_5 at the sides. The horn angle is 2ϕ. All distances are in micrometers, and the wavelength is 0.6328 μm.

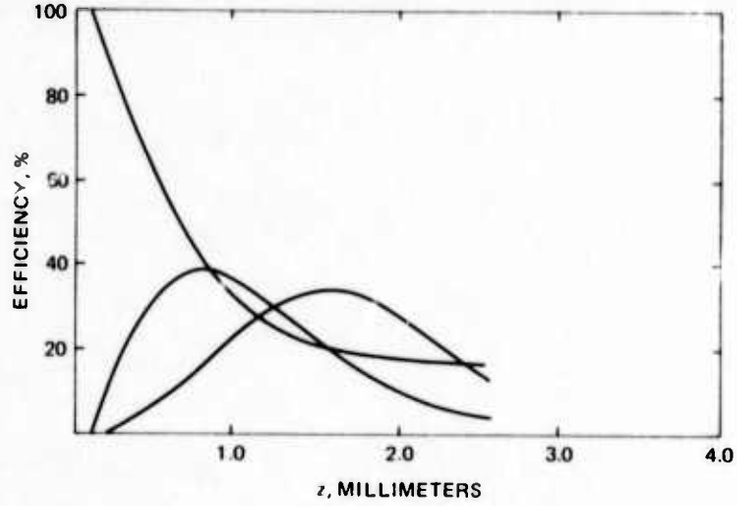

D

$\Phi = 1.5$
$t_y = 0.8\,\mu$
$n_1 = 2.22$
$n_2 = 1.0$
$n_3 = n_4 = n_5 = 2.2$
$t_x = 100\,\mu$ @ $z = 1.92$ mm

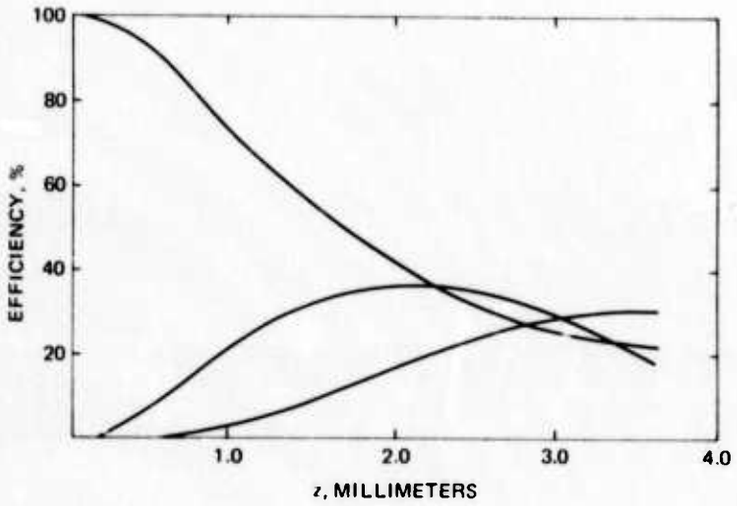

E

$\Phi = 1.0$
$t_y = 1.0\,\mu$
$n_1 = 2.22$
$n_2 = 1.0$
$n_3 = n_4 = n_5 = 2.2$
$t_x = 100\,\mu$ @ $z = 2.88$ mm

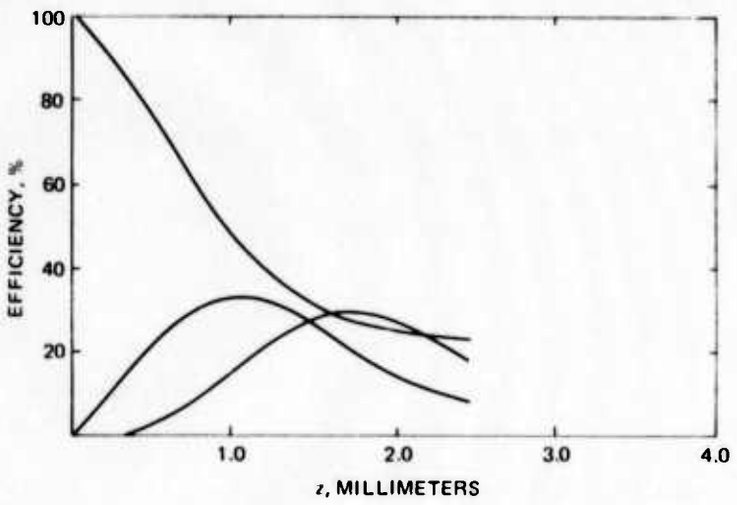

F

$\Phi = 1.5$
$t_y = 1.0\,\mu$
$n_1 = 2.22$
$n_2 = 1.0$
$n_3 = n_4 = n_5 = 2.2$
$t_x = 100\,\mu$ @ $z = 1.92$ mm

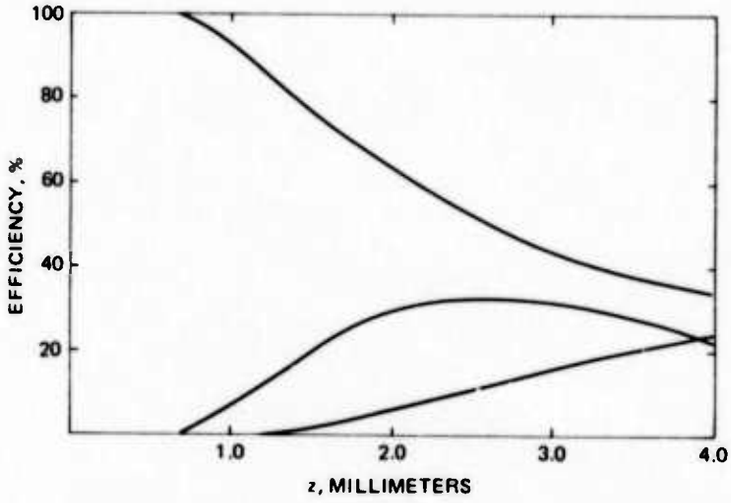

G

$\Phi = 1.0$
$t_y = 0.45\,\mu$
$n_1 = 1.57$
$n_2 = n_3 = n_5 = 1.0$
$n_4 = 1.53$
$t_x = 100\,\mu$ @ $z = 2.88$ mm

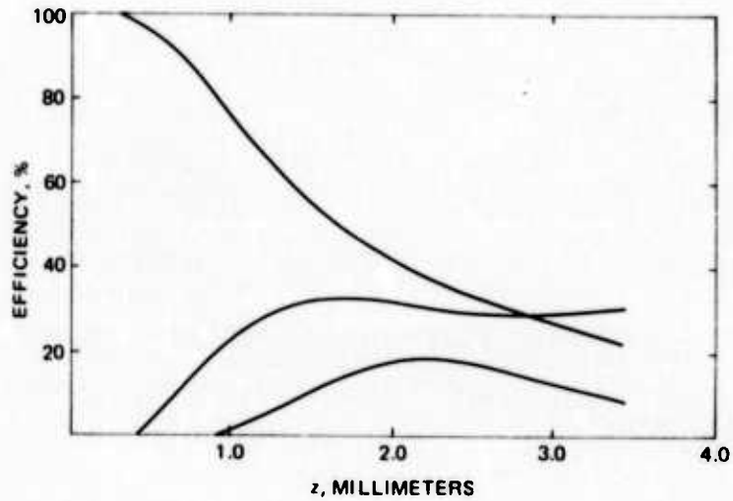

H

$\Phi = 1.5$
$t_y = 0.45\,\mu$
$n_1 = 1.57$
$n_2 = n_3 = n_5 = 1.0$
$n_4 = 1.53$
$t_x = 100\,\mu$ @ $z = 1.92$ mm

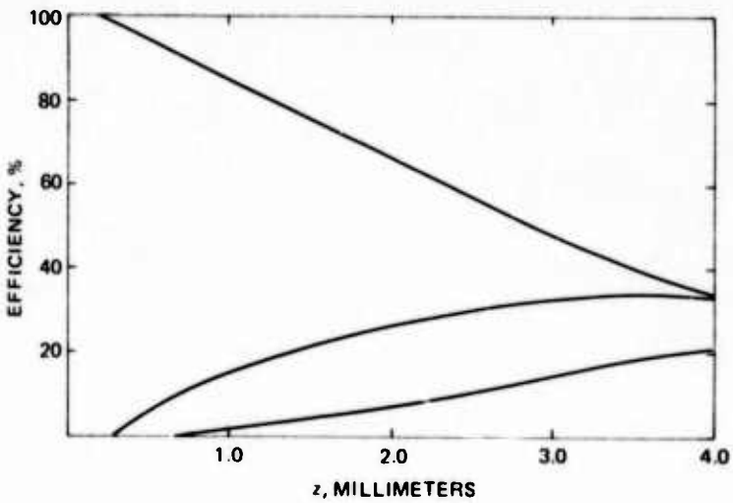

I

$\Phi = 1.0$
$t_y = 0.5\,\mu$
$n_1 = 1.57$
$n_2 = n_3 = n_5 = 1.0$
$n_4 = 1.53$
$t_x = 100\,\mu$ @ $z = 2.88$ mm

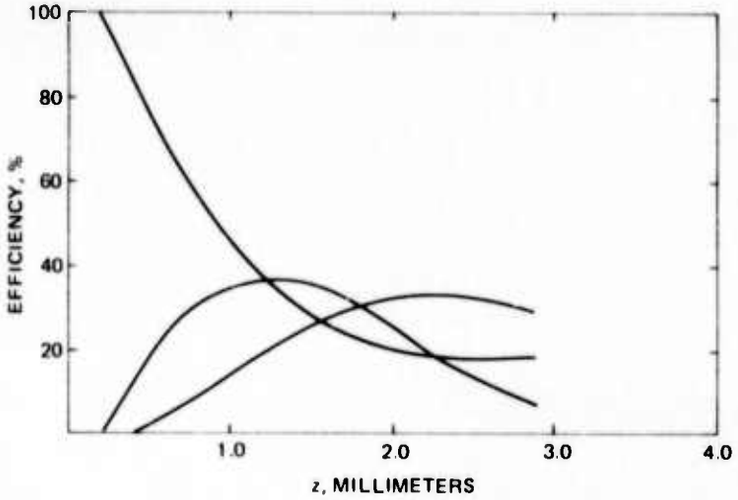

J

$\Phi = 1.5$
$t_y = 0.5\,\mu$
$n_1 = 1.57$
$n_2 = n_3 = n_5 = 1.0$
$n_4 = 1.53$
$t_x = 100\,\mu$ @ $z = 1.92$ mm

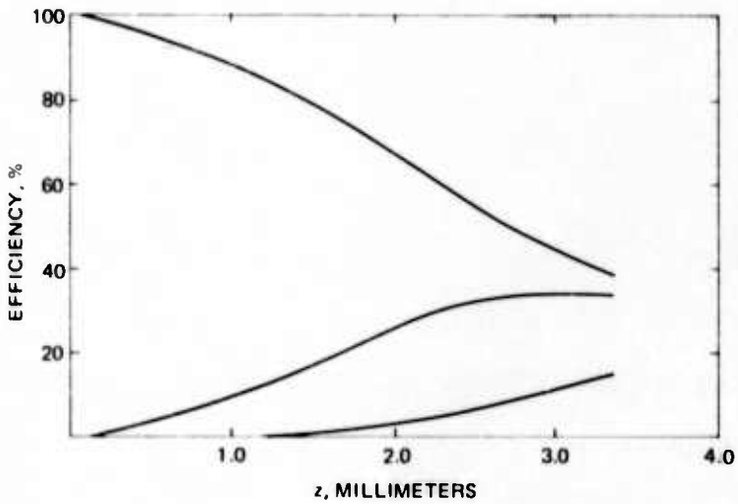

K

$\Phi = 1.0$
$t_y = 0.7\,\mu$
$n_1 = 1.57$
$n_2 = n_3 = n_5 = 1.0$
$n_4 = 1.53$
$t_x = 100\,\mu$ @ $z = 2.88$ mm

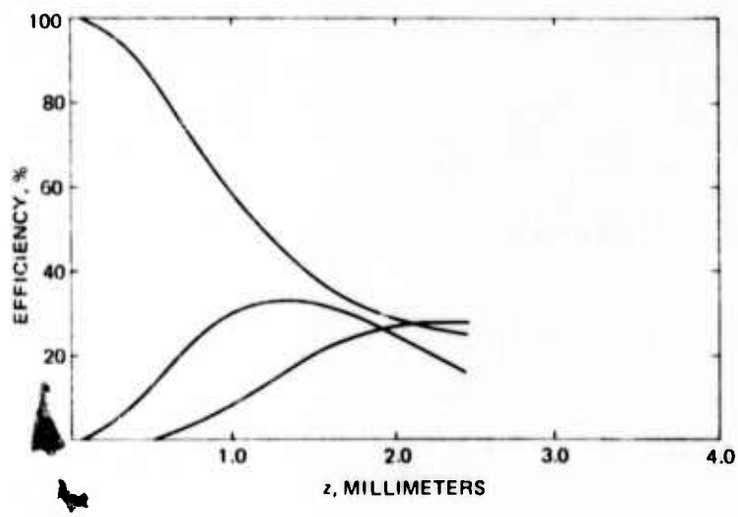

L

$\Phi = 1.5$
$t_y = 0.7\,\mu$
$n_1 = 1.57$
$n_2 = n_3 = n_5 = 1.0$
$n_4 = 1.0$
$t_x = 100\,\mu$ @ $z = 1.92$ mm

film and Gaussian in the other direction. The spatial distribution of the lowest-order guided mode $g_0(x,y)$ at the mouth of the horn is of modal character in both directions. These functions are well matched spatially and can be expected to yield a value for the integral in equation (1) that is close to unity. The integral is especially close to unity for guides of width large compared to the wavelength. The curves of the lowest-order mode in figure 3 may therefore be interpreted as the approximate coupling efficiency. The remaining curves may also be interpreted in terms of coupling efficiency, but their excitation requires that the incident beam be split so as to arrive from two different angles. Without splitting, the coupling efficiency for a higher-order mode is approximately one half that shown in the figures.

Mode conversion approximate coupling efficiency is shown for a waveguide of index n_1 embedded in a medium with n_2 above, n_4 below, and n_3 and n_5 on the sides. The aspect ratio is substantially larger than unity in each configuration. Two cases are treated. One case corresponds to a guide of index 2.22 embedded in a substrate of index 2.2 ($\Delta n = 1\%$). This configuration is intended as a model for a diffused waveguide. The other case is that of a guide of index 1.57 lying on a substrate of index 1.53. The parameters that are varied in the figures are the guide height (t_y) and the angle of the horn (ϕ is the half angle). Calculations for relatively shallow horn angles of 2° and 3° are shown.

The figures should be compared at a prescribed mouth width. The width is 100 μm for the 2° horn at a distance of 2.88 mm from the narrow end and for the 3° horn at a distance of 1.92 mm. Lesser and greater widths are found at proportional distances. The curves exhibit a diminution in power in the lowest-order mode that, while slow with respect to the wavelength, is rapid in terms of horn width. Typical efficiencies at widths of 100 μm are 40% or less. Higher-order modes are introduced at distances closer to the narrow end of the horn as the height of the guide is increased.

To interpret the behavior of the curves, we note that the power in the modes is computed as a solution to coupled equations of the form

$$\frac{d A_p}{dz} + i\beta_p e_z A_p = C_{pq}(z) A_q, \qquad (2)$$

where A_p is the amplitude, $\beta_p(z)$ is the varying guided mode propagation constant of the p^{th} mode, and $C_{pq}(z)$ is a coupling coefficient that also varies with z. The coefficient $C_{pq}(z)$ is zero until a horn width is reached at which a mode of order q can propagate. Once a new mode is introduced, the coupling coefficient takes on a peaked appearance with a relatively slow decay in z. The coupling coefficient is also proportional to the rate of expansion of the horn. The rate of coupling between modes p and q is dependent on the behavior of C_{pq} as well as the phase difference $\beta_p(z) - \beta_q(z)$. The smaller the phase difference, the more substantial the coupling. The phase difference and coupling coefficient amplitude effects compete, and a comparison of the relative power distribution among the modes in a horn of fixed angle may be seen to be a nonmonatonic function of the guide height t_y. The evolution of the power distribution in the modes with distance z resembles the Bessel function behavior of Raman-Nath diffraction. This is to be expected since the guided waves have small index differences.

There are a number of approximations that have been made to obtain the curves in figure 3. First, the guided modes have been approximated by

the product of TE and TM modal functions in the form[1,2]

$$g_n(x,y) = f_{o_{TE}}(x)\, f_{n_{TM}}(y), \tag{3}$$

where $f_{o_{TE}}(x)$ is the normalized solution for the tangential electric field of a planar guided TE mode, and $f_{h_{TM}}(y)$ is the electric field of a TM planar guided mode. Second, power coupling to the radiation spectrum has not been accounted for. Third, coupling to other mode orders as a result of bulk and surface imperfections has not been considered. The latter effect is doubtless the approximation least consistent with the physical situation. Scattering effects result in coupling between adjacent orders and can seriously degrade the coupling efficiency. This matter will be further examined in the future should horn structures be selected as a part of a coupling procedure. Radiation effects can be expected to be small for the shallow-angle horns considered here because of the substantial phase mismatch between the lowest-order guided mode and the unguided modes.

The objective of using the horn structure for coupling in linear guides is to reduce the accuracy requirement for aligning an input beam with the linear guide. For a uniform input beam of width L coupled to a uniform mode of the same width, a misalignment ΔL leads to power loss $\Delta L/L$. A misalignment in angle introduces significant power loss ($P = (2/\pi)^2$) when $\Delta\theta = \lambda/2L$. The product of positional and angular errors that lead to a power reduction to $(2/\pi)^2 = 0.405$ is found to be

$$\Delta\theta\ \Delta L = 0.3\lambda. \tag{4}$$

For nonuniform beams in which the fields are reduced toward the edge, the coefficient in front of λ in equation (4) is somewhat larger. The point in presenting equation (4) is to emphasize that while increasing the horn mouth reduces the tolerance requirement on ΔL, it increases the angular accuracy that is required.

From accuracy considerations as well as the curves of figure 3, we conclude that the use of simple horns is restricted to aperture widths that are substantially less than, for example, the 158-wavelength-wide horn that occurs at $t_x = 100\ \mu m$. If we consider the calculations for a waveguide ($n_1 = 2.22$) with 1% index difference at a height of 1 micrometer, a horn of 2% angle must be less than about 2/3 mm long (aperture size 23.3 μm) to achieve 90% theoretical coupling efficiency while a horn of 3% angle must be less than about 1/3 mm (aperture size 17.2 μm). Greater horn angles reduce the aperture size still further. The angular error that can be tolerated at these aperture sizes is less than 15 milliradians.

The straight-walled horn structure appears to be capable of playing only a limited role in improving coupling efficiency. Once the horn width reaches dimensions that can support many modes, the coupling efficiency is generally reduced below 50%. While wall tapering techniques,[3] which will be discussed in a later report on this contract, can be expected to offer some

[1] See references

improvement, the use of lensing methods appears to hold greater promise as a method for increasing aperture sizes by more than one order of magnitude. These methods will also be discussed in a future report.

ELECTRON BEAM MICROPROBE

A microprobe has been constructed to measure variations in the concentrations of the electrically active impurities in laser diodes and other semiconductor structures. In the microprobe the surface of the semiconductor is explored with a raster-scanned, focused beam of electrons. The scanning electron beam interacts with the specimen, generating localized light emission, changes in conductances, and induced currents and voltages. Any of these phenomena can be detected by an appropriate sensor. The sensor output modulates the intensity of the spot on an oscilloscope screen being scanned in a raster pattern in synchronization with the pattern scanned by the electron beam on the specimen. The oscilloscope then displays a magnified picture of the semiconductor surface as characterized by the particular phenomenon selected.

Classically, the electrically active impurity concentrations in semiconductors have been determined by means of electrical, galvanomagnetic Hall effect, and magneto resistance measurements. At best, such measurements provide averages over large areas of such material parameters as the charge carrier concentration, mobilities, and activation energies. Such measurements cannot determine these parameters on a microscopic scale or even for dimensions comparable to those of laser diode devices (of the order of 100 μm). The use of the scanning microprobe overcomes the dimensional limitations of the classical techniques.

Figure 4 illustrates the possible phenomena which can result from an electron beam incident on a semiconductor surface. It may generate heat, X rays, cathodoluminescence, induced currents and voltages, and secondary electrons. An appreciable fraction of the energy of the incident electron beam may be dissipated in the breaking of valence bonds and the generation of excess electron-hole pairs with an efficiency which for GaAs may be in excess of 30%. These electron-hole pairs have a finite lifetime before they recombine. A fraction of the electron-hole pairs will undergo recombination by giving up their excess energy in the form of light. This radiative recombination process is due to an electronic transition from the conduction band to the valence band, from impurity levels to the valence band, or from the conduction band to impurity levels. The spectral characteristics of the light output are a function of the donor and acceptor impurity type. The intensity of the light is a function of the impurity type, impurity concentrations, and the nature and characteristics of crystallographic lattice imperfections.

Figure 5 is a block diagram illustrating the basic concept of a scanning electron bombardment system suitable for electron microprobe investigations. It consists of an electron optical column, specimen chamber, signal collection system, and the electronics necessary to position the electron beam upon the sample and to display the resultant signal induced by the electron beam.

In the electron optical column, a beam of electrons from an electron gun is focused by the electron condenser lens and objective lens onto the

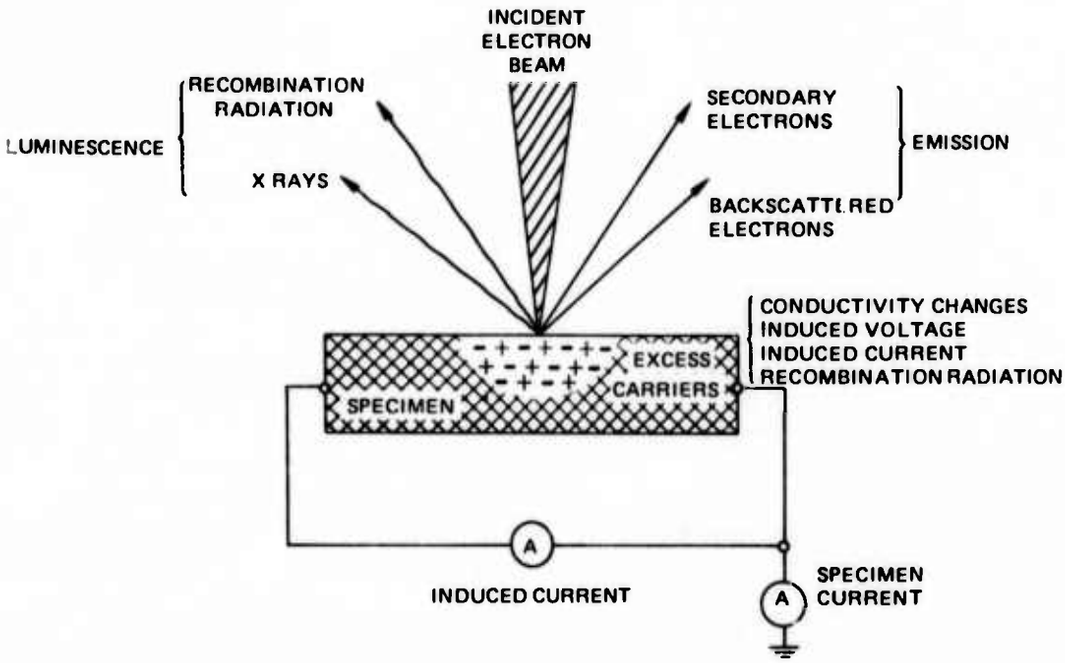

Figure 4. Electron beam induced phenomena.

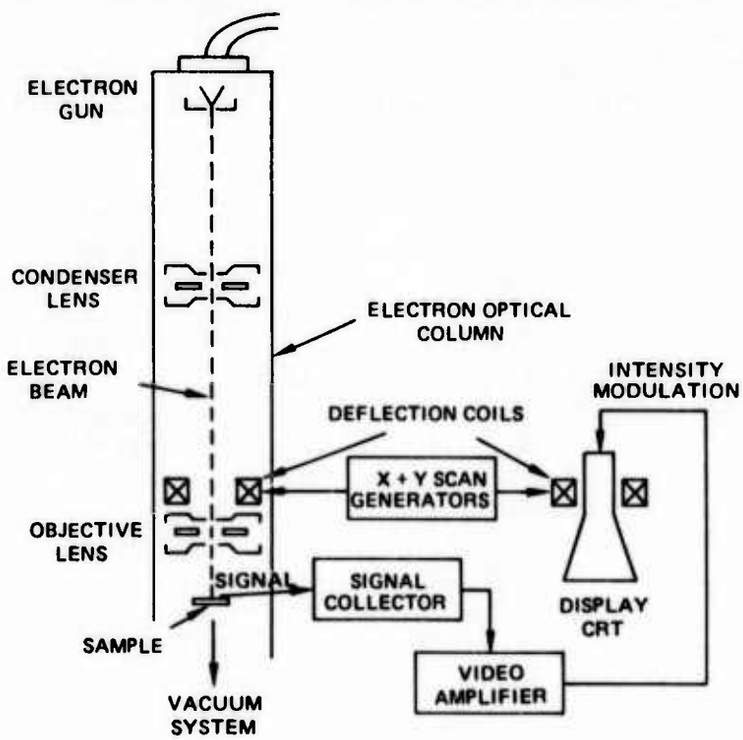

Figure 5. Scanning electron beam system.

specimen surface. A deflection system scans the beam across the specimen in a raster pattern when energized by suitable sawtooth waveforms from X and Y scan generators.

The net current flowing from a specimen of a particular geometrical configuration to ground is monitored by a lead attached to the sample; the sample in this case is isolated from ground. Also, the current induced in diodes by the injected electron beam can be monitored by grounding one diode lead and measuring the current in the circuit.

The cathodoluminescence collection optics consist of a spherical mirror mounted above the specimen and a 45° plane mirror below the specimen. The electron beam is incident upon the top surface of the specimen from above after passing through a hole in the center of the spherical mirror. Infrared radiation emitted by the spot on the sample bombarded by the electron beam is collected by the spherical mirror, which has an optical speed of f/2.3. The radiation is then reflected from the spherical mirror downward in a converging cone onto the 45° plane mirror, which reflects it out of the chamber through a vacuum-tight window which is transparent to the radiation of interest. For a GaAs sample the recombination radiation is then focused by a lens onto a PIN silicon photodiode. Alternatively, to obtain spectral information, the radiation is focused onto the entrance slit of a grating monochromator whose output is then monitored by the silicon detector.

The efficiency of recombination radiation induced by an incident electron beam is a function of the probability of radiative recombination over recombination by other processes. It is large in semiconductors such as GaAs in which electronic transitions occur with conservation of the k-vector and the conduction band minimum occurs at the same k-vector value as the maximum of the valence band. The local concentration of charge carriers directly affects the recombination probability; the diffusion of generated electron-hole pairs as well as the efficiency of their generation are important parameter attributes which determine the light output of homogenous GaAs.

First-order theoretical arguments suggest that the intensity of cathodoluminescence emission is proportional to the nonradiative lifetime and inversely proportional to the radiative lifetime of the charge carriers. The dependence of the intensity on the type, density, and spatial distribution of impurities can be inferred from their effects on the respective lifetimes and on the prevailing recombination mechanisms.

If an electron beam is scanned "edge on" across a GaAs p-n junction, then the induced electron-hole pairs, as well as the injected electrons, are affected by the electric field across the space charge region of width W. The generated excess holes will drift toward the p-side and electrons towards the n-side of the diode. If an external circuit is connected to the electrodes, then a current will flow in it. The magnitude of this current is a function of the relative position x_s of the beam with respect to the junction plane, the minority carrier diffusion lengths L_n and L_p, the charge carrier diffusion lengths L_n and L_p, and the charge carrier recombination velocities. Assuming an idealized point source on the surface, the charge collection efficiency Q is proportional to the current in the external circuit.

In principle, the minority carrier diffusion lengths can be determined from a measurement of the dependence of the p-n junction current on the

relative position x_s of the electron beam with respect to the junction plane, provided that such measurements are made over distances which are large with respect to the diffusion lengths.

Figure 6 shows experimental data obtained on a GaAs diode. A typical line scan "edge on" to the p-n junction produced the output current measured across a 10^3-ohm resistor as a function of the position of the incident electron beam relative to the junction plane. Assuming a relation of the form $i=i_o \exp(-x_s/L)$, the respective electron and hole diffusion lengths are $L_n=8.9\ \mu m$ and $L_p=5.4\ \mu m$, in good agreement with data obtained by other methods. From similar line scans, the local fluctuations L_n and L_p about a mean can be determined.

Figure 7 shows the cathodoluminescence emission as a function of position relative to the p-n junction plane of the same diode. With the electron beam moving from left to right, the emission rises towards a plateau which corresponds to a donor doping level of $\sim 5 \times 10^{17}\ cm^{-3}$. It rises steeply to a peak as the junction plane is approached and then decays abruptly to a minimum at the p-n junction plane. The reason for this minimum is probably the fact that as excess minority carriers generated by the electron beam drift across the junction, they become majority carriers in a time comparable to the relaxation time (which is much shorter than the radiative lifetime). For a point source of generated electron-hole pairs and spherical symmetry, and for constant radiative and nonradiative lifetimes, it might be expected that the cathodoluminescence output signal would be zero at the p-n junction plane. However, the intensity will not be zero at the junction if the source has a finite size; it will have a minimum value, approaching zero as the diffusion length becomes larger than the source size.

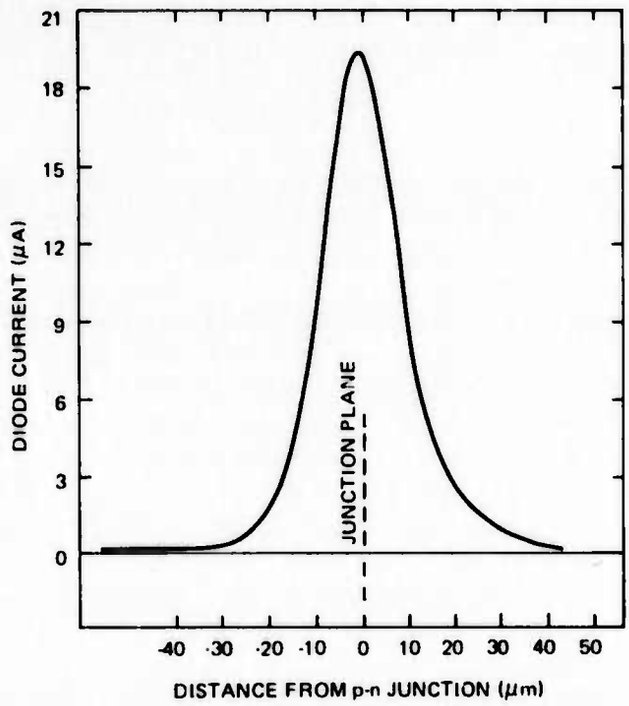

Figure 6. Line scan of electron beam induced diode current in GaAs LED.

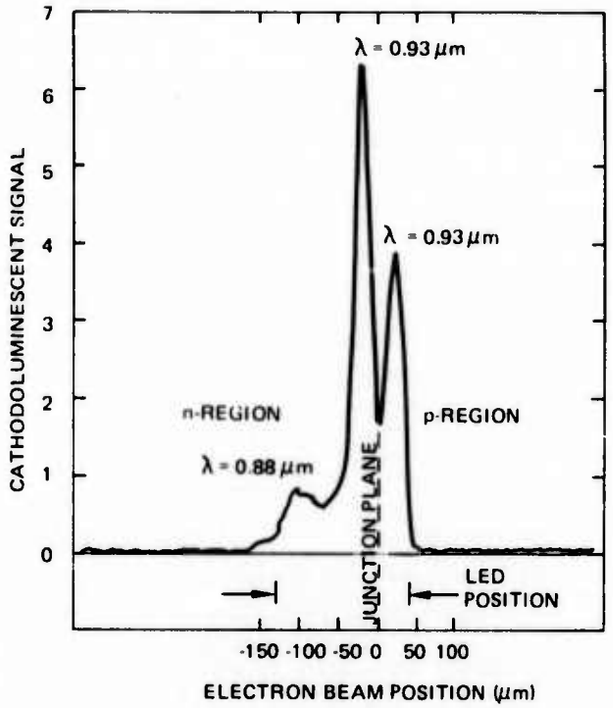

Figure 7. Cathodoluminescent line scan of GaAs light emitting diode.

APPARATUS FOR THE DETERMINATION OF THE REFRACTIVE INDEX OF THIN DIELECTRIC FILMS[4]

The method was suggested by Abeles[5] in 1950 and is based on Brewster's angle for determination of refractive index of thin transparent film deposited on a substrate. There were two reasons for setting up the apparatus: (1) For waveguiding to occur, the index of refraction n_1 of the confining medium must be larger than n_0 of the surrounding material. Further, the thickness of the guiding region should be of the order of λ. Therefore, methods to measure the index of refraction of this dielectric film are of considerable importance for IO. (2) For maximal coupling of light into the end of a waveguide, reflection losses must be small. Losses due to reflection can be reduced by deposition of an antireflection dielectric film of thickness $\lambda/4$. Obviously, for controlled deposition, thickness and refractive index of these layers must be measured.

THE APPARATUS

The apparatus for measuring the refractive index was designed so that the angle through which the detector moves is always twice the angle of incidence. This was done with a simple linkage system based on the fact that if a square is formed with four equal-length members pinned at their ends so that the square can be deformed by changing one of its corners to an acute angle, the diagonal moves through an angle which is just one half the angle

the adjacent side moves through. (See figure 8.) The movable arm on which the detector is mounted extends through the axis of rotation to a fixed scale. The position of the arm can be read to 10 minutes of arc, which means that the angle of incidence can be determined to 5 minutes. The movable arm reads zero on the scale when the angle of incidence is 45°. An optical bench is mounted on the main base so that the axis of the bench makes an angle of 90° with the center line of the movable arm when the arm is set at zero degrees. A He-Ne laser is mounted on the optical bench so that the beam is directed as accurately as possible along the axis of the bench.

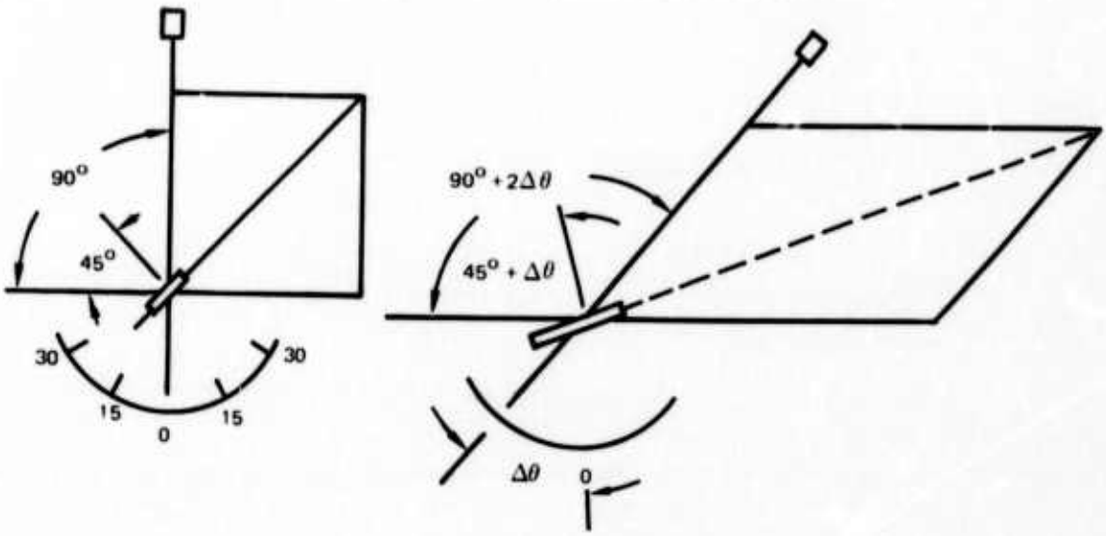

Figure 8. Geometry of apparatus.

If $\Delta\phi = 30°$, the angle of incidence is $45° + \frac{1}{2}\, 30° = 60°$.

The maximum accuracy of the refractive index of a substrate can be judged from the following table.

$\bar{\phi}_0$	$n_1 = \tan \bar{\phi}_0$
56° 20′	1.5013
56° 25′	1.5061
56° 30′	1.5108
56° 35′	1.5156

The reflection surface to be studied is attached to a Lansing Research Corporation mirror mount which in turn is attached to a Lansing translation stage. The latter device has a travel adjustment normal to the plane of the surface so that the axis of rotation can be adjusted to be in the plane of the surface. The above-mentioned translational stage is mounted rigidly to a second translational stage with the direction of travel parallel to the plane of the surface so that a substrate with a deposited film on part of the surface can be quickly shifted to permit comparison of reflections from bare substrate and film-covered substrate. The second translational stage is attached to the movable arm plate over the axis of rotation. The detector consists of a fiber optics probe (located in the plane of incidence) which guides the light to a

photomultiplier cell, all of which is part of Model 721 Linear Photometer of the Gamma Scientific Co. The probe is mounted on the end of the movable arm opposite the side of the axis of rotation from the angular scale.

ADJUSTING EQUIPMENT

The apparatus is mounted on a large flat stone surface. The plane of incidence is made horizontal by means of a metal plate with a small pinhole in it. The plate is supported from a stand which rests on the stone surface and is used in the following way. The plate is placed near the laser and the stand adjusted so that the light passes through the pinhole. The stand is then moved near to the detector and the mirror mount holding the reflecting surface is adjusted until the light passes through the pinhole in its new position.* Because of backlash in the instrument one must decide the direction of motion of the movable arm, either clockwise or counterclockwise, just before a reading is taken. A counterclockwise motion was used in these experiments. The fiber optics probe should then be clamped into position with the light centered on it. The translational stage just below the mirror mount is then adjusted so that the movable arm can be swung through its full range (counterclockwise) and the spot of light remains centered on the fiber optics probe throughout the range. If the plane of the reflecting surface does not include the axis of rotation, this will not be true, and the spot of light will not remain centered while the arm is moved through its complete range. As a preliminary adjustment the polarizer and analyzer are placed side by side in front of the laser and with the analyzer set at 0° the polarizer is adjusted for extinction of the light. The light through the polarizer is then in the plane of incidence (E_p). The polarizer is then turned through a degree or two so some small E_s will be incident on the reflecting surface. The analyzer is then moved to its regular position in front of the detector.

If the laser beam is lined up accurately with the axis of the optical bench and the probe is lined up with the axis of the movable arm for an angle of incidence equal to the Brewster angle, the minimum of the reflected intensity will occur with the analyzer at 90° and the movable arm angle will yield the correct angle of incidence. If the laser beam is not lined up along the axis of the optical bench, the movable arm will not indicate the correct Brewster angle. This is so because the reflecting surface can be adjusted to send the

*The above-mentioned adjustment may require a motion of the fiber optics probe in the vertical direction. The probe should be centered along the axis of the movable arm in the horizontal plane.

reflected beam into the fiber optics probe when the movable arm reads zero, but the angle of incidence may not be 45°. See figure 9.

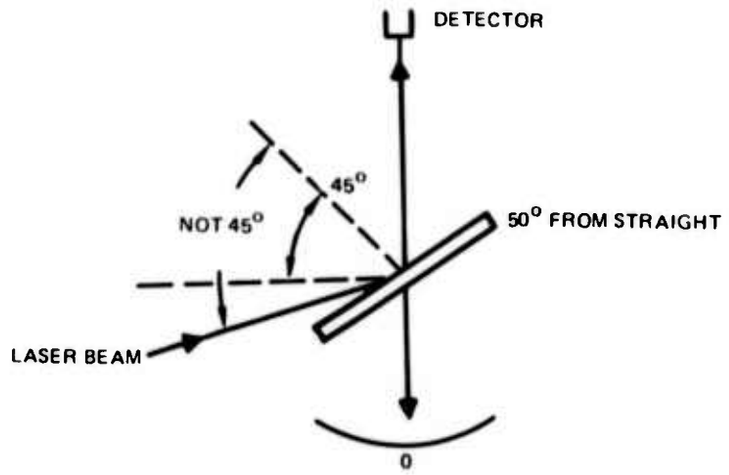

Figure 9. Geometry with laser beam out of line.

In a case of this kind the movable arm reading will not give the correct Brewster angle when the minimum for the light reflected from a bare substrate is found for the analyzer at 90°. One can make a correction for the angle of incidence by using a reflecting surface of known refractive index and determining the movable arm reading when the minimum intensity occurs for the analyzer set at 90°. When the refractive index is known, from the Brewster angle relationship, one knows the true angle of incidence ($\phi_0 = n_1$). The difference between the measured angle and the true angle $\Delta\phi$ must then be added to or subtracted from the 45° in the expression so that

$$\phi_0 = (45° \pm \Delta\phi) + \frac{\theta_{MA}}{2},$$

where θ_{MA} is the movable arm reading for the analyzer at 90°.

It was found possible, however, to adjust the direction of the laser beam so that the movable arm reading did give a value of the refractive index very close to the known value.

Some results are shown in figures 10 – 12.

The ZnSe substrate shown in figure 11 reduced the normal reflectance from a single surface of ZnSe (back surface blackened) from approximately 20% to 3%.

In order to obtain the refractive index of a substrate, a rough determination of the Brewster angle should be made. This can be done by setting the analyzer at 90° and noting the minimum response of the photometer when the movable arm is turned through a wide angle. The readings of the analyzer for a minimum response are only meaningful in the vicinity of the Brewster angle.

Although the equations which have been presented in this report were based on the assumption that we were dealing with an infinitely thick substrate

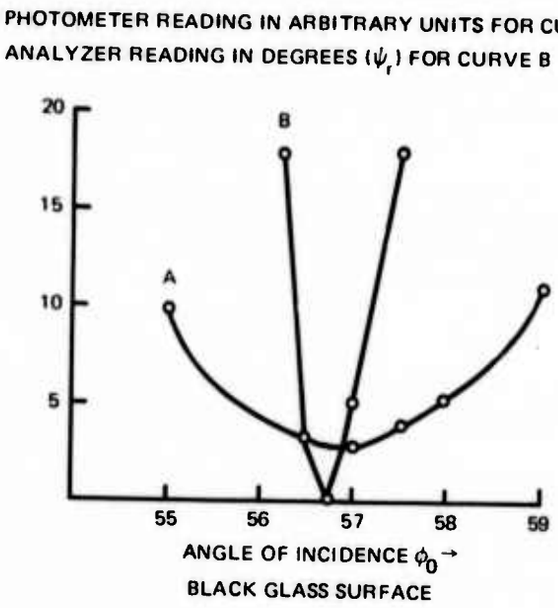

Figure 10. A comparison between data taken without the analyzer and data taken by recording the position of the analyzer when set for a minimum. The data were taken on a UV filter (black glass). The use of the analyzer results in a sharp V-shaped curve. The minimum occurs at $\phi_0 = 56^\circ\, 45'$. The tangent of this angle is 1.525, which is the refractive index of the glass.

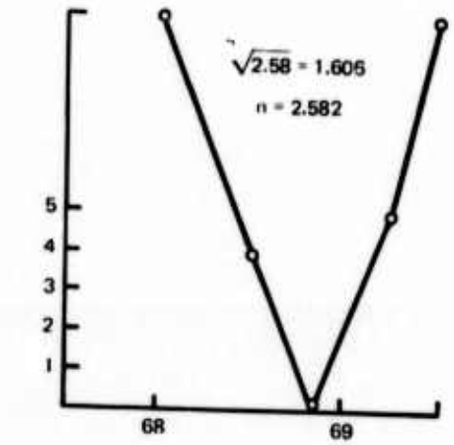

Figure 11. Plot of data taken for a bare surface of ZnSe. The position of the analyzer for minimum transmission is plotted against the angle of incidence. The minimum occurs at $\phi_0 = 68^\circ\, 50'$, from which the refractive index is seen to be $n_1 = 2.582$.

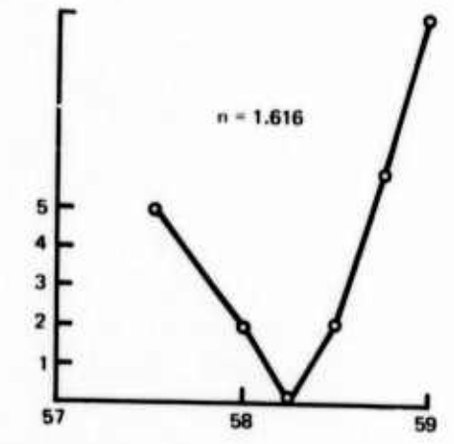

Figure 12. Data taken on a ZnSe substrate a portion of which was overlaid with a thin film produced by the evaporation of SiO_2. The analyzer reading obtained for the same intensity reflected from substrate and film-coated substrate is plotted against the angle of incidence. The minimum in the curve occurred at $58^\circ\, 15'$. The tangent of this angle is 1.616, which is the refractive index of the film.

(no reflections from the back surface), the results are also applicable to substrate of finite thickness. Data taken for a blackened back surface were essentially the same as for an unblackened back surface. The latter did not give as deep a minimum (zero) at the Brewster angle. The Brewster angle for the back surface is far removed from that of the front surface – something like 33° compared to 56° for glass. The method of determination of the refractive index herein described is dependent on the change of phase of R_p at the Brewster angle, and this is of interest only at the front surface. What happens at the back surface is too far removed to be of interest.

CW LASER-FABRICATED CHANNEL ACTIVE AND PASSIVE OPTICAL WAVEGUIDES

An optical waveguide confines (guides) light, in function being similar to a microwave waveguide. The light is confined in the dielectric by multiple internal reflections. As mentioned, the prerequisite for confinement is that the index of refraction n_1 of the guiding dielectric must be greater than the index n_0 of the surrounding material. Further, the angle of incidence θ must be greater than the critical angle.

IO is still in its early stages. Practical applications of IO devices depend to a large extent on convenient methods for producing channel (three dimensional) waveguides. One of the major problems in the fabrication of channel waveguides is their size. They must be of the order of λ and possess smoothness to the order of about a tenth of λ to minimize losses.

Some of the methods employed to produce channel waveguides are the following:

1. Ion bombardment (ion implantation) of fused quartz is one of the earliest methods for obtaining three-dimensional waveguiding.[6,7] Of newer date is ion implantation in semiconductors.[8] This method produces a refractive index change of low loss.

2. Rf sputtering employing suitable glasses results in low-loss channel waveguides.[9]

3. Embossing grooves in a plastic material forms dielectric channel waveguides. The grooves are filled with polymethylmethacrylate, which is later polymerized.[10]

4. Photolithographic techniques are used to obtain waveguide structures on semiconductors.[11,12] Changes in the refractive index n of the waveguide are achieved by a diffusion process. For example, the index of refraction of ZnSe (n_{ZnSe}) is increased by diffusing CdSe into it, since $n_{CdSe} > n_{ZnSe}$.

5. Electrochemically induced migration of ions into glass[13] has been used recently to produce channel waveguides.

A new method for producing channel waveguides, described below, allows us to produce channel waveguide structures in both passive and active dielectric substrates.

PASSIVE CHANNEL WAVEGUIDES

The beam of a Spectra Physics Model 164 argon ion cw laser is focused with the aid of a microscopic objective onto the surface of a piece of a highly absorbing glass. Jena glass filters OG 550 and OG 590 proved very suitable. These filters absorb the $\lambda = 4880$ Å line (and shorter wavelengths) of the argon ion cw laser very efficiently, but have high transmission for red and infrared light. At the focal point of the microscopic objective, glass is evaporated. If the glass piece is moved at constant speed (100 μm/sec) perpendicularly to the laser beam, very smooth grooves are produced. The smallest groove produced which exhibits waveguiding was about 1.6 μm wide. However, grooves about 2–4 μm wide and 4–12 μm deep are the most convenient to produce. The depths of these grooves were estimated from interferometric observations. These observations also indicate that the grooves have very shallow walls. This supports the assumption that the glass has been evaporated, rather than melted.

Originally it was intended to fill the grooves with a liquid (or plastic) which had a higher refractive index n than that of the filter glass. However, rather strong waveguiding was observed under the grooves, without any filling.

We conclude that the high temperature created at the focal point of the laser beam evaporates some glass. Further, the high temperature also causes some composition changes in the unevaporated material around the groove. The change in composition must produce a slight increase in the index of refraction of the glass surrounding the groove. The observed optical guiding is rather strong. With the method just described, it should be possible to fabricate couplers, frequency selective structures, and other passive elements. At present, the mounting stage is being equipped with a fine micrometer screw, to allow the placement of grooves parallel to each other with an error of about ± 0.2 μm. This accuracy is required for the quantitative demonstration of optical coupling between two grooves.

ACTIVE CHANNEL WAVEGUIDES

Active devices such as modulators and switches are important for IO circuitry. These devices operate on the electrooptical effect. The index of refraction n of a semiconductor material is changed by the application of an electric field. This change in n can then be used to produce modulation of phase and/or amplitude of a guided light beam in a channel waveguide.

The cw laser line of an argon ion laser at 4880 Å (as well as the shorter ones) is very strongly absorbed by CdS and ZnSe. Because of this, grooves 6 – 8 μm wide were produced in slabs of single crystals in these materials. Rather leaky waveguiding was observed around the grooves. This led to the conclusion that the heat produced at the focal point on the surface of the semiconductor, besides evaporating some of the material, induces a lowering of the index of refraction around the grooves. In order to fabricate waveguides employing this effect, one simply uses a biepitaxial slab of semiconducting material ($n_1 > n_2$). Two grooves in the top material (n_1), several μm apart, are produced. Waveguiding is observable between the grooves.

A biepitaxial slab of ZnSe, ZnSeTe ($n_{ZnSe} < n_{ZnSeTe}$) on GaAs was used. Two grooves which were separated by about 15 μm from each other were produced in the ZnSe (top) layer. Strong waveguiding was observed in the area confined by the two grooves.

To fabricate a modulator, several grooves were made on the slab at different distances. Then a film of SiO_2, followed by an Al film, was deposited on the top of the slab. Basically, the arrangement was the same as described in reference 14. An ac voltage was applied between the GaAs and the Al film. A phase shift was observed, indicating modulation.

SUMMARY

The advantages of fiber optics for many military applications are well established. Channel optical waveguides in turn are the backbone of IO. Passive IO elements such as lenses, gratings, couplers, and frequency mixers and active IO elements such as detectors, sources (for example, semiconductor lasers), modulators, and switches can be interconnected or combined to fabricate IOCs.

Consequently, considerable NELC effort in IOCs has centered around the fabrication of channel waveguides and methods to measure parameters on waveguides which determine optical guiding. In particular, the following studies were performed.

1. Diffusion masks were fabricated by Hughes Research Laboratories employing a scanning electron microscope. The masks were produced by exposure of photo resist on a SiO_2 layer on ZnSe substrates by the electron beam.

2. A theoretical study on the efficiency of coupling to optical waveguides with linearly tapered horns was carried out. It was found that straight-walled horn structures seem to be capable of improving coupling efficiencies to some degree. It was also concluded that the lensing method appears to hold greater promise for efficient coupling.

3. Changes in the concentration of electrically active impurities in semiconductors (for example, laser diodes) were determined with the aid of an electron beam microprobe. The surface of the specimen was investigated with a focused beam of electrons. The scanning electrons interact with the semiconductor and produce X rays, cathodoluminescence, induced currents and voltages, secondary electrons, etc. Through the use of proper detectors, the modulated intensities are displayed on an oscilloscope screen, which shows a magnified picture of the semiconductor surface. The picture on the oscilloscope is characteristic for the phenomenon selected by use of the particular detector.

From experiments on GaAs light emitting diodes employing the electron beam microprobe, mobilities and other parameters which characterize semiconductor devices can be obtained. These data can also be determined with the aid of the classical methods, such as galvanomagnetic Hall effect, magnetoresistance, and other electrical measurements. However, these measurements give only averages over large areas. The advantage of the scanning electron beam microprobe results from its capability to provide these

data from measurements on devices of very small dimensions, such as active IO devices.

4. An apparatus for the measurement of refractive index of thin dielectric films was constructed. A detailed derivation was given, which relates measured parameters to basic principles (Maxwell's equations). The equipment, together with the derivations, should be very useful in determining the refractive index of dielectric films and semiconductor surfaces having small changes in their refractive index (channel waveguides).

5. By focusing an argon ion cw laser with the aid of a microscopic objective onto the surface of a moving piece of highly absorbing glass, low-loss channel waveguides were produced. At the laser focal point, glass is evaporated, producing grooves 2–10 μm wide. Similarly, by focusing the laser beam on an epitaxial layer of ZnSe on GaAs, small grooves are fabricated. However, waveguiding occurs only between two grooves.

REFERENCES

1. E. A. J. Marcatilli, Bell Systems Technical Journal, 48, 2071 (1969)

2. J. E. Goell, Bell Systems Technical Journal, 48, 2133 (1969)

3. R. P. Hecken and A. Anuff, IEEE Trans. MTT, 21, 374 (1973)

4. J. J. Brady, NELC TN 2503 (24 October 1973). (The theoretical portion of this TN is duplicated on page 21 of this report. NELC TNs are informal documents intended chiefly for use within NELC.)

5. F. Abeles, J. Phys. Rad., 11, 310 (1950)

6. E. R. Schineller, R. P. Flam, and D. W. Wilmot, J. Opt. Soc. Am., 58, 1171 (1968)

7. R. D. Standley, W. M. Gibson, and J. W. Rodgers, Appl. Opt., 11, 1313 (1972)

8. E. Garmire, H. Stoll, A. Yariv, and R. G. Hunsperger, Appl. Phys. Letters, 21, 87 (1972)

9. J. E. Goell and R. D. Standley, Bell Syst. Tech. J., 48, 3445 (1969)

10. R. Ulrich, H. P. Weber, E. A. Chandross, W. J. Tomlinson, and E. A. Franke, Appl. Phys. Letters, 20, 213 (1972)

11. H. F. Taylor, W. E. Martin, D. B. Hall, V. N. Smiley, Appl. Phys. Letters, 21, 95 (1972)

12. W. E. Martin and D. B. Hall, Appl. Phys. Letters, 21, 325 (1972)

13. T. Izawa and H. Nakagome, Appl. Phys. Letters, 21, 584 (1972)

14. W. E. Martin, J. Appl. Phys., 44, 3703 (1973)

APPENDIX: INTEGRATED OPTICS REPRINTS, TALKS, AND PUBLICATIONS

1. H. F. Taylor, W. E. Martin, V. N. Smiley, and D. B. Hall, "Fabrication of Optical Circuits by Solid State Diffusion," OSA Topical Meeting on Integrated Optics, Las Vegas, 7 February 1972

2. H. F. Taylor, W. E. Martin, D. B. Hall, and V. N. Smiley, "Fabrication of Single Crystal Semiconductor Waveguides by Solid State Diffusion," Appl. Phys. Lett., 2195 (1972)

3. W. E. Martin and D. B. Hall, "Optical Waveguides by Diffusion in II-VI Compounds," Appl. Phys. Lett., 21, 325 (1972)

4. H. F. Taylor, V. N. Smiley, W. E. Martin, and S. S. Pawks, "Fluorescence of Graded-Band-Gap CdS_xSe_{1-x} Crystals Produced by Diffusion," Phys. Rev., B.5, 1467 (1972)

5. D. B. Hall and W. E. Martin, "Diffused Optical Waveguides in II-VI Compounds," Quantum Electronics Conference, Montreal (1972)

6. D. B. Hall and C. Yeh, "Leaky Waves in A Heteroepitaxial Film," J. Appl. Phys., 44, 2271 (1973)

7. H. F. Taylor, "Optical Switching and Modulation in Parallel Dielectric Waveguides," J. Appl. Phys., 44, 3257 (1973)

8. H. F. Taylor, "Frequency Selective Coupling in Parallel Dielectric Waveguides," Opt. Comm., 8, 421 (1973)

9. W. E. Martin, "Photoluminescence Determinations of Cd Diffusion in ZnSe," J. Appl. Phys., December 1973

10. W. E. Martin, "Waveguide Electro-Optic Modulation in II-VI Compounds," J. Appl. Phys., 44, 3703 (1973)

11. C. Elachi and C. Yeh, "Frequency Selective Coupler for Integrated Optics Systems," Opt. Comm., 7, 201 (1973)

12. H. F. Taylor, "Optical Modulation in Thin Films," J. Vac. Science and Technology, January-February 1974

13. H. F. Taylor, "Fiber Optics Communications," Naval Research Review, January 1973

14. H. F. Taylor, "Power Loss at Directional Change in Dielectric Waveguides," Applied Optics (to be published April 1974)

15. M. K. Barnowski, "Electron and Ion Beam Microfabrication," chapter 7, Introduction to Integrated Optics, ed., Plenum Press (to be published)